Acta Oceanol. Sin., 2024, Vol. 43, No. 8, P. 128–141
https://doi.org/10.1007/s13131-024-2302-2
http://www.aosocean.com
E-mail: ocean2@hyxb.org.cn

Morphological, phylogenetic and metabolite profile of *Prorocentrum clipeus*, a newly recorded epiphytic dinoflagellate in the northern Yellow Sea

Ruifang Wang[1, 2], Mengmeng Tong[1], Shiwen Zhou[3], Junjie Zheng[2], Wenguang Zhang[1], Xinfeng Dai[2], Douding Lu[2], Jiarong Hu[2], Tianze Leng[2], Qinglin Mu[4], Zhongyong Yan[4], Jiangning Zeng[1, 2*], Pengbin Wang[1, 2*]

[1] Ocean College, Zhejiang University, Zhoushan 316021, China

[2] Key Laboratory of Marine Ecosystem Dynamics, Second Institute of Oceanography, Ministry of Natural Resources, Hangzhou 310012, China

[3] The State Key Laboratory of Marine Pollution, Department of Biomedical Sciences, City University of Hong Kong, Hong Kong SAR 999077, China

[4] Zhejiang Marine Ecology and Environment Monitoring Center, Zhoushan 316000, China

Received 4 October 2023; accepted 29 February 2024

Abstract

More than 30 species of benthic *Prorocentrum* have been identified, some of which produce okadaic acid (OA) and its derivatives, dinophysistoxins (DTXs), which cause diarrhetic shellfish poisoning (DSP). Increasing numbers of benthic *Prorocentrum* species have been reported in tropical and subtropical waters of China. In contrast, only a few benthic *Prorocentrum* species have been reported in temperate waters. In this study, morphological descriptions obtained using light microscopy, scanning electron microscopy and molecular characterization of one *Prorocentrum clipeus* strain isolated from the Yellow Sea are presented. *Prorocentrum clipeus* cells were nearly circular in shape, with a collar, ridge, and one protrusion. The periflagellar area was wide U-shaped, with two curved projections on platelet 1a. Nine periflagellar platelets of different sizes were observed. The morphology closely fits that of the species isolated from other locations. Phylogenetic analysis based on the molecular sequences of the small subunit (SSU) rDNA, internal transcribed spacer (ITS), and large subunit (LSU) rDNA was performed. A comprehensive metabolomic analysis incorporating target, suspect and non-target screenings was first applied to investigate the intracellular and extracellular metabolite profiles of the current isolate of *P. clipeus*. According to the results of the target and suspect screenings, 179 metabolites or toxins produced by DSP-related algal species, including OA, dinophysistoxin-1 (DTX1), dinophysistoxin-2 (DTX2) and pectenotoxin-2 (PTX2), were not detected. Non-target screening involving feature-based molecular networking (FBMN) provided a global view of major metabolites produced by the *P. clipeus* DF128 strain and revealed 23 clusters belonging to at least 13 compound classes, with organometallic compounds, lipids and lipid-like molecules, phenylpropanoids and polyketides, and benzenoids as major types. To date, this is the first record of the characterization of *P. clipeus* in samples from Chinese waters. Our results support the wide distribution of epibenthic *Prorocentrum* species.

Key words: *Prorocentrum*, taxonomy, phylogeny, metabolite profiling, Yellow Sea

Citation: Wang Ruifang, Tong Mengmeng, Zhou Shiwen, Zheng Junjie, Zhang Wenguang, Dai Xinfeng, Lu Douding, Hu Jiarong, Leng Tianze, Mu Qinglin, Yan Zhongyong, Zeng Jiangning, Wang Pengbin. 2024. Morphological, phylogenetic and metabolite profile of *Prorocentrum clipeus*, a newly recorded epiphytic dinoflagellate in the northern Yellow Sea. Acta Oceanologica Sinica, 43(8): 128–141, doi: 10.1007/s13131-024-2302-2

1 Introduction

The dinoflagellate genus *Prorocentrum* was erected by Ehrenberg (1834), with *Prorocentrum micans* as the type species (Ehrenberg, 1834). Since then, more than 80 species have been described (Arteaga-Sogamoso et al., 2023; Chomérat et al., 2019; Gómez et al., 2023; Hoppenrath et al., 2013; Luo et al., 2017; Tillmann et al., 2023a, 2023b; Zou et al., 2020). Species of the genus are widely reported in tropical and temperate waters, where they occur in benthic, epibenthic and planktonic habitats. Approximately 36 of these species are associated with benthic habitats, such as sediments, and live epiphytically on macroalgal surfaces, floating detritus and corals (Arteaga-Sogamoso et al., 2023; Chomérat et al., 2019; Hoppenrath et al., 2013, 2014; Lim et al., 2019). To date, ten benthic species (e.g., *Prorocentrum caipirignum* S. Fraga, M. Menezes & S. M. Nascimento, *Prorocentrum concavum* Y. Fukuyo, *Prorocentrum foraminosum* M. A. Faust, *Proro-*

Foundation item: The National Natural Science Foundation of China under contract Nos 41706191 and 41961144013; the Natural Science Foundation of Zhejiang Province under contract No. LY20D060004; the National Natural Science Foundation of China under contract Nos 41676111, 41876139 and 41906140; the Program of Bureau of Science and Technology of Zhoushan Grant under contract No. 2019C81031; the Basic Public Welfare Research Project of Zhejiang Province under contract No. LGC22B050032.
*Corresponding author, E-mail: jiangningz@126.com; algae@sio.org.cn

centrum hoffmannianum M. A. Faust, *Prorocentrum leve* M. A. Faust, Kibler, Vandersea, Tester & Litaker, *Prorocentrum lima* (Ehrenberg) F. Stein, *Prorocentrum porosum* Arteaga-Sogamoso et al. & Mancera-Pineda and *Prorocentrum rhathymum* A. R. Loeblich Ⅲ, Sherley & R. J. Schmidt) have been reported to produce diarrheic shellfish toxins (DSTs), okadaic acid (OA) and its methyl derivatives dinophysistoxins (DTXs) (Arteaga-Sogamoso et al., 2023; Glibert et al., 2012; Hoppenrath et al., 2013; Nascimento et al., 2017; Verma et al., 2019). These toxins can accumulate in shellfish, mainly bivalve mollusks, and the consumption of these seafoods by humans causes diarrhea shellfish poisoning (DSP), accompanied by symptoms such as diarrhea, nausea, vomiting and abdominal pain (European Food Safety Authority, 2008; Yasumoto et al., 1985).

Morphologically, *Prorocentrum* species are bilateral thecate flagellates with 2 apical heterodynamic flagella. The useful characters for differentiation at the species level include cell shape and size, thecal surface, pore patterns, intercalary band and the periflagellar area. The morphology of the periflagellar area is based on several features, e.g., flagellar pore, accessory pore, collar, ridge, wing, protrusion, platelet lists, curved projections, and spines; all of these features were comprehensively reviewed by Hoppenrath et al. (2013) and Tillmann et al. (2019). Numerous studies have revealed the high diversity of *Prorocentrum* species based on morphological characteristics and molecular phylogenetic data. Several new species of *Prorocentrum* have been described in recent decades (Arteaga-Sogamoso et al., 2023; Chomérat et al., 2010, 2011; Faust et al., 2008; Gómez et al., 2023; Grzebyk et al., 1998; Han et al., 2016; Henrichs et al., 2013; Hoppenrath, 2000; Hoppenrath and Leander, 2008; Lim et al., 2019; Murray et al., 2007; Ten-Hage et al., 2000; Tillmann et al., 2023a, 2023b). A comparison revealed species complexes in the genus *Prorocentrum*, such as the *P. lima/P. caipirignum* complex, the *P. concavum/P. foraminosum* complex, the *P. emarginatum/P. fukuyoi* complex and the *P. rhathymum* complex (Chomérat et al., 2019).

Previous studies revealed that there are several benthic *Prorocentrum* species in China, such as *P. lima* from the South China Sea, which has a very high degree of morphological and genetic variability. Morphological and molecular data revealed five morphotypes of *P. lima* from Hainan Island, labeled morphotypes 1, 2, 3, 4 and 5 (Zhang et al., 2015). Furthermore, morphotype 4 was identified as *P. caipirignum* by Nascimento et al. (2017). Seven *Prorocentrum* species, *P. lima*, *P. rhathymum*, *P. concavum*, *Prorocentrum* cf. *emarginatum*, *P. fukuyoi*, *P.* cf. *maculosum* (synonymized with *P. caipirignum* by Nascimento et al. (2017) and *Prorocentrum panamense,* have been described after isolation from the northern South China Sea, and OA was detected in all the strains of *P. lima* and *P. caipirignum* (Luo et al., 2017). Six benthic species from the tropical Zhongsha Islands have also been reported, including *P. concavum, P.* cf. *sculptile*, *P. emarginatum*, *P. hoffmannianum*, *P. lima*, and *P. rhathymum* (Xie et al., 2022). Seven *Prorocentrum* species were identified in the Xisha Islands, including *P. borbonicum*, *P. caipirignum*, *P. concavum*, *P. elegans*, *P.* cf. *emarginatum*, *P. lima* complex, and *P. rhathymum* (Zou et al., 2022). Among these species, *P. borbonicum* and *P. elegans* were recorded in Chinese waters for the first time. In the Yellow Sea, East China Sea and South China Sea, four benthic species were identified, namely, *P. concavum*, *P. fukuyoi*, *P. mexicanum* and *P. tsawwassenense* (Wu et al., 2022). The increasing reports of novel potentially toxic *Prorocentrum* species in tropical and subtropical waters in China have raised concerns about their potential impact on marine ecosystems and public health. However, the majority of these studies on *Prorocentrum* were conducted in the South China Sea, leaving the other sea areas of China largely underexplored.

In this study, one newly recorded benthic *Prorocentrum* isolated from the Yellow Sea was identified as *P. clipeus* via morphology and phylogeny. To evaluate the potential of this species of algae for DSP or other toxicity, the metabolite profile of the obtained *P. clipeus* strain was systematically explored by employing an integrated metabolite profiling method involving target, suspect, and non-target screening via liquid chromatography coupled with mass spectrometry (LC-MS). PTXs, a group of polyether toxins, are non-diarrheagenic and are found only in some *Dinophysis* species but may co-occur with DSTs (Blanco et al., 2005). Accordingly, pectenotoxin-2 (PTX2) was selected for target screening. *Prorocentrum* and *Dinophysis* can both produce OA and DTXs, implying that they may share the same or similar OA and DTX biosynthesis systems. The toxins and metabolites from both species were evaluated via suspect screening (Jackson et al., 1993; Freudenthal and Jijina, 1988).

2 Materials and methods

2.1 *Isolation and culture*

Sand samples were collected on January 24, 2019, from Qingdao, Shandong, in the Yellow Sea (36°5′24″ N, 120°27′57.6″ E). Single cells of the target *Prorocentrum* were isolated and washed in K-Si medium (Keller et al., 1987) under an Olympus CKX53 inverted microscope (Olympus, Japan) via the capillary pipette method (Andersen, 2005). Then, the isolated cells were cultured in 96-well plates containing 200 μL of K-Si medium supplemented with local seawater that had been filtered (Glass-fiber filter, Waterman, UK) and autoclaved. When a sufficient cell density was achieved, the cells were transferred to 25 mL tissue flasks (Thermo Fisher Scientific, USA). The strain was cultured in fresh K-Si medium at approximately 20-day intervals to maintain culture health. The algae were maintained at (22 ± 2)℃ with a light: dark cycle of 12 h:12 h [100–150 μmol/(m^2·s); cool white fluorescent tubes] (Han et al., 2016).

2.2 *Light microscopy and laser scanning confocal microscopy*

Live and fixed cells were observed using an inverted microscope (CKX53, Olympus, Tokyo, Japan). Cell measurements were determined by light microscopy using a digital camera (SC180, Olympus, Tokyo, Japan) at 400× magnification. All the results were based on measurements of more than 50 randomly selected cells. Cell length was estimated from the anterior end to the posterior end in the valve view, and cell width was estimated as the trans-diameter in the lateral view. The periflagellar numbering system followed the labeling system proposed by Hoppenrath et al. (2013).

The nucleus, chloroplast and cell wall of *P. clipeus* were observed via laser scanning confocal microscopy (LSCM) (Leica Microsystems CMS GmbH, TCS SP5 Ⅱ, Mannheim, Germany). Chloroplasts were observed in glutaraldehyde-fixed cells at an excitation wavelength of 488 nm and emission wavelengths of 672–750 nm at 400× magnification using Leica Application Suite Advanced Fluorescence v 2.6.4.8702. The shape and location of the nucleus were determined by staining glutaraldehyde-fixed cells for 10 min in 1×SYBR® Green Ⅰ (Sigma-Aldrich, USA) at the final concentration and photographed at an excitation wavelength of 488 nm and an emission wavelength of 505–562 nm. For epifluorescence, the cells were stained with 1% Calcofluor White (Sigma-Aldrich, USA) and examined under ultraviolet light

at 405 nm excitation and 410–472 nm emission.

2.3 *Scanning electron microscopy*

Live samples in mid-exponential batch cultures were fixed with 4% glutaraldehyde (Sigma-Aldrich) at 4℃ for 4 h. The samples were then filtered through polycarbonate membrane filters (diameter 13 mm, pore size 3 μm; Whatman, Little Chalfont, United Kingdom), washed with distilled water to completely remove all fixation reagents and sea salt, dehydrated at graded concentrations [10%, 30%, 50%, 70%, 90%, 95%, 100% (three times)] of ethanol for 15 min each step, critical point-dried with a CO_2 Critical Point Dryer [model: HCPD-15-100, Joel Hi-Tech (Dalian) Co. Ltd., China], and coated with gold–palladium in an MSP-1S sputtering device (Vacuum Device, Ibaraki, Japan). Micrographs were taken using an M-1000 Tabletop microscope (Hitachi High-Technologies Corporation, Japan) and Zeiss Ultra 55 field-emission SEM (Zeiss, Jena, Germany).

2.4 *DNA extraction, PCR amplification, and sequencing*

Total genomic DNA was extracted from clonal cultures in the mid-logarithmic growth phase (30 mL) using a MiniBEST Universal DNA Extraction Kit (Takara, Tokyo, Japan) according to the manufacturer's protocol. For PCR amplification, primers (Table 1) were combined with nuclear small subunit rDNA (SSU), internal transcribed spacer (ITS), and large subunit rDNA (LSU). PCR was performed on SSU rDNA using TaKaRa EX Taq^R (TaKaRa, Japan) in a total volume of 30 μL. The amplification conditions for SSU rDNA were as follows: initial 5 min denaturation step at 95℃; 35 cycles of denaturation at 95℃ for 30 s, annealing at 52℃ for 30 s and extension at 72℃ for 1 min for 30 s; and a final elongation cycle of 72℃ for 10 min. The PCR mixture (20 μL) of ITS1-5.8S-ITS2 and LSU rDNA consisted of 6 μL of double-distilled water, 10 μL of 2× TSINGKE^R Master Mix (blue) (TSINGKE, China), 2 μL of primer (1 μL of forward primer and 1 μL of reverse primer) and 2 μL of template. The thermal cycling procedure was 4 min at 94℃; 39 cycles of 20 s at 94℃, 40 s at 52℃, and 1 min at 72℃; and a final extension of 10 min at 72℃. A Thermal Cycler (T100^{TM} Thermal Cycler; Bio-Rad, Hercules, CA, USA) was used for all PCRs. Labeled DNA fragments were analyzed by capillary electrophoresis on an ABI 3730xl Genetic Analyzer (Applied Biosystems). Editing and contig assembly of rDNA sequence fragments were carried out using Sequencher v5.4.5 (Gene Codes Corporation). The sequences were deposited in GenBank under accession numbers OP601437.1, OP601439.1 and OP601441.1.

2.5 *DNA sequence comparisons and phylogenetic analyses*

Phylogenetic analyses inferred from SSU rDNA, ITS1-5.8S-ITS2 rDNA and LSU rDNA were performed separately. The sequences of the strain were aligned with sequences of other *Prorocentrum* species retrieved from GenBank. The sequences were aligned using ClustalW (Thompson et al., 1994), a portion of the BioEdit program v7.0.5.3 (Hall, 1999). Poorly aligned positions and divergent regions were trimmed to the same length, and the gaps were deleted. Sequence differences and similarities were obtained within a DNAStringSet from a FASTA file using the Biostrings package in R (version 4.3.1). The *P. clipeus* DF128 sequences were subjected to a BLAST search against the GenBank database (http://www.ncbi.nlm.nih.gov/blast) to test for sequence homology with nontarget taxa. The sequences of the strains in each dataset were analyzed via two methods of phylogenetic reconstruction: maximum likelihood (ML) using Mega-X software (http://www.megasoftware.net) and Bayesian inference (BI) using MrBayes V.3.2.1 (Ronquist et al., 2012). The most suitable model of substitutions was first selected using the software MrModelTest2.3 and PAUP*4.0b10 (Swofford, 2002). For the SSU matrix, the ITS alignment and the LSU matrix, the general time reversible model (GTR+I+G) was chosen, as indicated by the Akaike information criterion (AIC) and Bayesian information criterion (BIC) tests implemented in MrModelTest2.3.

ML phylogenetic trees were constructed with 1 000 bootstrap replicates. Bootstrap values (>50) are indicated at each branch node. For BI analysis, the Markov Chain Monte Carlo (MCMC) process was set to four chains, and 5 000 000 generations were run. The sampling frequency was set to every 100 generations. Following analysis, the standard deviation of the frequencies was confirmed to be <0.01, the first 25% of all the trees were discarded (burn-in), and a consensus tree was constructed from the remaining trees. A Bayesian posterior probability (BI) (>0.50) is indicated at each branch node.

2.6 *Metabolite profiling*

2.6.1 *Sample preparation*

Algal cells were collected by filtration with a 47 mm Isopore PC membrane (10 μm pore size, Merck Millipore). The cell pellet was transferred to a tube and extracted with 20 mL of methanol (Knowles, China) under ultrasonication at 50% amplitude for 2 min in pulse mode (6 s work/3 s interval, 130 W, 220 V) until completely broken to collect the cell extract solution (JY92-IIN, Xinzhi, China). The solution was subsequently centrifuged at 12 000 r/min for 5 min to collect the supernatant, which was dried using nitrogen gas flow to obtain the cell extract solution. The lysate was dried by evaporation under a gentle stream of high-purity nitrogen. The algal crude extracts were subjected to liquid-liquid partitioning using n-hexane and 90% aqueous

Table 1. Primer sequences used to amplify the SSU, ITS and LSU rDNA regions in *Prorocentrum* species

Name	Target sequence	Direction	Sequence (5′ to 3′)	Reference
18F23	SSU	forward	GGTTGATCCTGCCAGTAG	Olmos-Soto et al. (2002)
18R1780	SSU	reverse	GTTCACCTACGGAAACCTTG	Fu et al. (2008)
SR4-F 548-566	SSU	forward	AGGGCAAGTCTGGTGCCAG	Hong et al. (2008)
SR5kawR 630-611	SSU	reverse	ACTACGAGCTTTTTAACCGC	Hong et al. (2008)
SR6-F 891-910	SSU	forward	GTCAGAGGTGAAATTCTTGG	Hong et al. (2008)
SR7-R 951-932	SSU	reverse	TCCTTGGCAAATGCTTTCGC	Hong et al. (2008)
SR9-R 1 286-1 267	SSU	reverse	AACTAAGAACGGCCATGCAC	Hong et al. (2008)
ITS1-F	ITS1-5.8S-ITS2	forward	TCCGTAGGTGAACCTGCGG	White et al. (1990)
ITS4-R	ITS1-5.8S-ITS2	reverse	TCCTCCGCTTATTGATATGC	White et al. (1990)
DIR	LSU	forward	ACCCGCTGAATTTAAGCATA	Scholin et al. (1994)
D2C	LSU	reverse	CCTTGGTCCGTGTTTCAAGA	Scholin et al. (1994)

methanol three times at a volume ratio of 1:2 to afford two fractions. The 90% MeOH layer was dried with a rotatory evaporator and then redissolved in dichloromethane and 60% aqueous methanol three times at a volume ratio of 1:1 to afford two fractions. Each fraction was dried by evaporation under a gentle stream of high-purity nitrogen. The two fractions were then redissolved in 1 mL of methanol, filtered through a 0.22 μm membrane nylon (66) into a liquid chromatography injection vial, and stored at –20℃ for mass spectrometric analysis.

The culture filtrate was filtered with a C18 solid-phase extraction (SPE) cartridge to collect the extracellular extract. An SPE device was installed in a fume hood. Three milliliters of chromatographically pure methanol were added to Oasis hydrophilic-lipophilic balance (HLB) cartridges (200 mg, 3 mL; Waters, USA), after which the mixture was allowed to flow slowly; this process was repeated once. Next, 3 mL of ultrapure water was slowly allowed to flow through to rinse away residual methanol; this process was repeated once. The filtrate was added, and extraction was performed at a flow rate of 1 mL/min. After the sample passed through the extraction column and while it was still wet, ultrapure water was added to rinse the wall of the SPE column until it became completely dry. Next, the SPE column was rinsed with methanol, and approximately 10 mL of eluent was collected. The eluent was then dried using nitrogen gas. Liquid-liquid extraction was then performed by the same procedure described for the algae cells. The procedural blank samples (i.e., extraction without actual sample) were also prepared and analyzed to filter out any contaminants that might have been introduced during sample preparation.

2.6.2 *Ultra-performance liquid chromatography-QTRAP analysis*

The standards and samples were analyzed using an Agilent 1290 Infinity Ultra-Performance Liquid Chromatograph (UPLC, Palo Alto, CA, USA) interfaced with a Sciex 5500 QTRAP mass spectrometer (Foster City, CA, USA) for target analysis. The flow rate of the mobile phases was 0.2 mL/min. The column oven temperature was set at 40℃. The injection volume was 5 μL. Milli-Q water was the aqueous mobile phase and 95% acetonitrile/Milli-Q water (95:5, *v*/*v*) was the organic mobile phase, both of which contained 0.1% formic acid and 2 mmol/L ammonium formate. A Phenomenex Kinetex C18 analytical column (100 × 2.1 mm i.d., particle size 1.7 μm) was used to separate the analytes. The LC gradient program started at the 20% organic mobile phase and was maintained for 1 min, after which it was increased to the 80% organic mobile phase within 5 min and maintained for 2 min. Afterward, it was increased to the 100% organic mobile phase within 2 min and maintained for 4 min before returning to the 20% organic mobile phase within 0.1 min. The column was equilibrated at the initial gradient condition for 4.9 min prior to the next sample injection.

Target analytes were detected using multiple reaction monitoring in both positive and negative electrospray ionization (ESI) mode. The ESI parameters were set as follows: positive ion-spray voltage, 5 500 V; negative ion-spray voltage, –4 500 V; curtain gas, 10 psi (14.5 psi = 1 bar); GS1, 30 psi; GS2, 40 psi; ion source temperature, 400℃; and collision gas, medium. Nitrogen served as the collision gas in both modes. Two standards were selected for quantification and confirmation. The detailed chemical formula, MS/MS parameters, and retention times of the standards are listed in Table 2. The acquired data were processed using Sciex Analyst software (version 1.63; Foster City, CA, USA).

2.6.3 *Ultra-performance liquid chromatography-QTOF HRMS analysis*

The UPLC-QTOF system was used for suspect and non-target screenings of analytes. The separation of analytes was conducted using an Agilent 1290 Infinity Ⅱ UPLC system (Agilent, Palo Alto, CA, USA) equipped with the same C18 analytical column. The QTOF unit was operated in both positive and negative electrospray ionization (ESI) mode. The flow rate of the mobile phases was 0.2 mL/min. The column oven temperature was set at 40℃. The injection volume was 10 μL. Milli-Q water was the aqueous mobile phase, and 95% acetonitrile/Milli-Q water (95 : 5, *v*/*v*) was the organic mobile phase; both of these phases contained 0.1% formic acid and 2 mmol/L ammonium formate for positive ESI mode and only 2 mmol/L ammonium formate for negative ESI mode. The LC gradient program started at the 20% organic mobile phase, was maintained for 1 min, was increased to the 100% organic mobile phase in 20 min and was maintained for 10 min before being returned to the 20% organic mobile phase in 0.1 min. The column was equilibrated at the initial gradient condition for 3.9 min prior to the next sample injection.

HRMS screening was performed on a Sciex X500R mass spectrometer system (Foster City, CA, USA). Dynamic background subtraction was applied to the information-dependent acquisition (IDA) criteria for dynamic exclusion in high-resolution mode. The TOF-MS mass used was 100 Da to 2 000 Da (250 ms for each analysis per cycle), and the TOF-MS/MS mass used was 50 Da to 2 000 Da (100 ms for each analysis per cycle) for both positive and negative ESI modes. The fragment ions were generated from collision induced dissociation with nitrogen under a standardized collision energy (CE) (30 V) with collision energy spread (CES) (15 V) in positive ESI mode and CE = –30 V with CES = 15 V in negative ESI mode. The other detailed parameters of the QTOF unit were set as follows: curtain gas, 30 psi; GS1, 40 psi; GS2, 40 psi; CAD gas, 7 psi; ion source temperature, 500℃ for both positive and negative ESI modes; ion spray voltage, 5 500 V; declustering potential, 80 V; collision energy, 30 V for

Table 2. Mass spectrometric parameters and retention times of the OA, DTX1, DTX2 and PTX2 standards

Compound	Molecular formula	Precursor ion type	Precursor ion (*m*/*z*)	Fragment ion (*m*/*z*)	DP/V	EP/V	CE/eV	CXP/V	Retention time/min
OA	$C_{44}H_{68}O_{13}$	$[M-H]^-$	803.5	255.2*	–70	–10	–60	–12	7.45
				113.1^	–70	–10	–75	–12	7.45
DTX1	$C_{45}H_{70}O_{13}$	$[M-H]^-$	817.5	255.2*	–110	–10	–68	–12	8.57
				113.1^	–110	–10	–94	–12	8.57
DTX2	$C_{44}H_{68}O_{13}$	$[M-H]^-$	803.5	255.2*	–70	–10	–60	–12	7.72
				113.1^	–70	–10	–75	–12	7.72
PTX2	$C_{47}H_{70}O_{14}$	$[M+NH_4]^+$	876.4	823.5*	150	10	27	15	7.94
				805.5^	150	10	35	15	7.94

Note: *, quantificationion; ^, confirmationion.

positive ESI mode; ion spray voltage, −4 500 V; declustering potential, −80 V; and collision energy, −10 V for negative ESI mode. Nitrogen served as the collision gas in both modes.

2.6.4 *Suspect screening*

For the suspect screening, an in-house compound library comprising 179 reported compounds was constructed using the library module in SCIEX OS software (version 3.16) and used as a suspect screening list (Fig. 1). These 179 reported compounds were summarized by referring to reported metabolites from the DSP-related species *Prorocentrum* spp. and *Dinophysis* spp. in SciFinder^n. During the suspect screening, the features, including the m/z of the ion adducts ($[M+H]^+$, $[M+NH_4]^+$, $[M-H]^-$), isotope pattern, and MS/MS (MS^2) fragments of the samples, were compared against the suspect screening list.

2.6.5 *Non-target screening*

The feature-based molecular network was developed from UPLC-HRMS/MS data (in positive and negative ESI modes) for non-target screening (Nothias et al., 2020). First, the raw MS/MS data files, including those from the OA, dinophysistoxin-1 (DTX1), dinophysistoxin-2 (DTX2) and PTX2 standards, were converted to 64-bit mzML files with the MSConvert program (version 3.0, Proteowizard®) (Holman et al., 2014). The converted mzML files were then imported to the MZmine program (version 3.4.27) for feature detection via the following steps: mass detection, chromatogram building, chromatogram deconvolution, isotopic grouping, retention time alignment, blank removal, and missing peak filling. Mass detection was performed by keeping the noise level at 8E1 for MS^1 and 5 for MS^2 in negative ESI mode and 5E2 for MS^1 and 8E1 for MS^2 in positive ESI mode in a mass spectrometer (Schmid et al., 2023). The processed data were submitted to the Global Natural Product Social (GNPS) platform to generate an FBMN (Gurevich et al., 2018; Mohimani et al., 2018). Subsequently, the obtained molecular network was enhanced via network annotation propagation in GNPS using the MolNetEnhancer workflow to enhance chemical structural annotation (Ernst et al., 2019). Cytoscape (version 3.10.0) was used to visualize and analyze the resulting molecular network (Shannon et al., 2003). OA [CRM-OA-d, (8.4 ± 0.4) μg/mL], DTX1 [CRM-DTX1-c, (7.8 ± 0.5) μg/mL], DTX2 [CRM-DTX2-b, (3.8 ± 0.2) μg/mL] and PTX2 [CRM-PTX2-b, (4.40 ± 0.13) μg/mL] were purchased from the National Research Council Institute for Marine Biosciences (Halifax, NS, Canada).

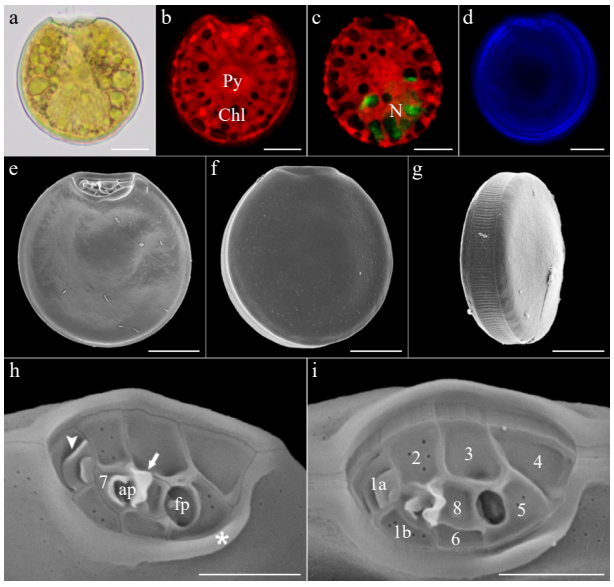

Fig. 1. Light microscopy (LM) and scanning electron microscopy (SEM) images of *P. clipeus* DF128. Light microscopy, right thecal view showing the cell shape, the large nucleus (N) posterior (a). Laser scanning confocal microscopy images of *P. clipeus* (b–d). Epifluorescence image showing the pyrenoid (Py) and radial arrangement of chloroplasts (Chl) (b). Sybr Green stained cell showing the shape of the nucleus (N) (c). Epifluorescence image of the thecal valve of the cell (d). The right valve view shows that the cell shape is asymmetrical and round (SEM) (e). Left valve view showing the smooth thecal surface with a radial pore pattern (SEM) (f). The intercalary band is wide and has transverse striation (SEM) (g). The cell is shown in the right lateral view, with a wide arc-shaped periflagellar area. Ridge (asterisk), wing-shaped protrusion (arrow), curved projections (arrowhead), detail of the nine platelets (SEM) (h and i). Scale bars in a–g: 10 μm, h and i: 5 μm.

3 Results

3.1 *Morphology—Prorocentrum clipeus Hoppenrath 2000*

The cells are nearly round and dorsoventrally flattened (Fig. 1a). The cells are 37.8–41.3 μm long and 35.7–39.7 μm wide. The length-to-width ratio varies from 1.00 to 1.09 (n = 50) (Fig. 1a). The cell has asymmetrical valve margins with a rounded anterior and posterior, and it is broadest in the middle (Figs 1e and f). Golden-brown chloroplasts containing a large internal pyrenoid are observed below the two valves in the cell center, and they presumably conduct photosynthesis for the cell (Figs 1a and b). The large kidney-shaped nucleus is situated at the posterior end of the cell (Figs 1a and c).

In the apical region, the left valve is slightly indented, whereas the right valve shows obvious dents (Figs 1e and f). The right valve forms a wide U-shaped depression in the periflagellar area (Fig. 1e). The left thecal plate has a collar at the anterior end (Fig. 1f). Wing-shaped protrusion, ridge and curved projections are observed in the apical area (Figs 1e, h and i). The surfaces of both thecal plates are smooth with scattered pores, which are absent in the central area of the thecal surface. The pores are very small, and some cells exhibit a pore pattern or radial rows over the thecal plates (Figs 1e and f). Small pores are randomly distributed in the platelets. There are no marginal pores. The intercalary band is granulated and transversely striated; it is narrow in new cells but wider in older cells (Fig. 1g).

The periflagellar area consists of a cluster of nine platelets around two pores, the smaller accessory pore (ap) and the larger flagella pore (fp). The platelet formula is 1a, 1b, 2, 3, 4, 5, 6, 7, 8 (Figs 1h and i), following the labeling system of Hoppenrath et al. (2013). The flagellar pore (fp) is oval and adjacent to platelets 3, 5, 6 and 8. The ap is surrounded by platelets 2, 6, 7 and 8. Four platelets (1a, 2, 3, 4) border the anterior valve (Figs 1h and i). The periflagellar platelet 1a is quadrilateral and adjacent to platelets 1b, 2, and 7. Two curved projections are observed on the dorsal side of platelet 1a. Platelet 2 is quadrilateral and touches the accessory pore. Platelet 3 is pentagonal and adjacent to one side of the flagellar pore. Platelet 4 is triangular and abuts two thecal plates, platelets 3 and 5, and it does not touch the flagellar pore. Platelet 5 is elongated and bends to form most of the right side of the flagellar pore when viewed from the right valve. Platelet 6 is adjacent to one side of the flagellar pore and to platelets 1b and 8. Platelet 7 is elongated and bends to form most of the left side of

Table 3. Comparison of the morphological features of *Prorocentrum clipeus* and similar benthic *Prorocentrum* species

Characteristic	*P. clipeus* (this study)	*P. clipeus*[1]	*P. clipeus*[2]	*P. compressum*[5]	*P. tsawwassenense*[7]	*P. panamense*[8]
Cell shape	nearly round	nearly round	nearly circular	ovate to rotundate	oval	heart-shaped
Cell size						
Length/μm	37.8–41.3	54–55	37–55 (37–44)[3]; (30–35)[4]	30–50 (35–50)[6]	40–55	46–52 (52.3–55.6)[9]
Width/μm	35.7–39.7	50–52.5	32–36.5[4]	C. 25(20–30)[6]	30–47.5	43–46 (48.3–50.7)[9]
L/W	1.00–1.09	1.05–1.08	?	?	?	1.06–1.13[9]
Periflagellar area						
Shape	wide U-shaped	wide arc-shaped	wide U-shaped (arc)	slight depression	wide U-shaped	linear
Collar on left plate	Yes	Yes	Yes	No?	Yes	No
Ridge on right plate	Yes	Yes	Yes?	No	No	No
Wing-shaped spine	No	No	No	Yes	"Yes" protrusions	No
Protrusions						
Only one	Yes	"Yes" apical spine	Yes	?		No
More than one				?	5 (6)[2]	No
Platelet list(s)	No	No	No	?	No	No
No. of platelets	9	10	9	?	7-9 (8-10)[2]	? 9[9]
Flagellar pore	Yes	Yes	Yes	?	Yes	Yes
Accessory pore	Yes	Yes?	Yes?	?	Yes[2]	Yes
Theca ornamentation	smooth	smooth	smooth	foveate[6]	smooth	areolate (reticulate-foveate)[2, 9]
Pore pattern	Yes, some cell visible pore pattern or radial rows	No, *scattered*	No visible pore pattern or radial rows of small pores (radial rows)[3]	No, scattered (rows of pores)[6]	Radial rows Two apical rows	No, scattered on valves, mostly around
Platelet pores	Yes	Yes	Yes?	?	No	No
Marginal pores	No	No	?	?	Yes	? No[5]
Plate center	Devoid	Devoid	?	Yes?	Devoid	? (Devoid in some cells)[2]
Large pores/μm	No	No	?	?	0.3–0.5	No
Small pores/μm	Approximately 0.15 μm in diameter	Approximately 0.12 μm in diameter	?	?	0.09–0.17	0.15
Intercalary band	Transverse striation	Smooth	? (horiz. str.)[3]	?	Transverse and horizontal striation	Transversally striated
Pyrenoid	Yes (LSCM)	Probably yes (LM)	?	?	Yes (TEM)	Yes
Nucleus (shape and position)	Large kidney-shaped, Posterior	Large kidney-shaped, Posterior	Kidney-shaped, Posterior	?	Round to oval, Posterior	U-shaped, Posterior

Note: In the above table, the list of morphological features was made based on Hoppenrath et al. (2013). It is listed here with some modifications, where notifications in the table indicate: ? = no data available; · · · ? = not mentioned in the text, inferred from images. Literature: [1]Hoppenrath (2000); [2]Hoppenrath et al. (2013); [3]Murray (2003); [4]Shah et al. (2013); [5]Dodge (1975); [6]Gul and Saifullah (2011); [7]Hoppenrath and Leander (2008); [8]Grzebyk et al. (1998); [9]Luo et al. (2017).

the accessory pore. The accessory and flagella pores are separated from each other by platelet 8. A detailed view of the periflagellar area shows one conspicuous protrusion formed by platelet 8 next to the accessory pore (Figs 1a, h and i). The ridge (asterisk) on the right thecal plate at the edge of the periflagellar area is shown in Fig. 1h.

3.2 *Phylogenetic analysis*

Molecular analysis confirmed the identification of the DF128 strain in this study as *P. clipeus*. The phylogenetic trees generated through ML and BI analyses exhibited congruent topologies. The topologies of the ML and BI trees based on the SSU, ITS/5.8S, and LSU rDNA gene sequences were most similar. Hence, only the topologies of the ML phylogenetic trees are shown (Fig. 2 for SSU, Fig. 3 for ITS/5.8S, and Fig. 4 for LSU rDNA).

According to the analysis based on the SSU alignment (Fig. 2), *P. clipeus* neighbored two other clades. One clade included *P. micans*, *P. koreanum*, *P. rhathymum*, *P. tsawwassenense*, *P. triestinum*, *P. donghaiense*, *P. minimum*, and *P. compressum*; the other clade included *P. panamense*, *P. pseudopanamense* and *P. glenanicum*. *Prorocentrum fukuyoi* and *P. emarginatum* formed the sister clade to this group. These species neighbored one clade, formed with *P. cassubicum* and *P. sipadanese*. All of the above species were planktonic and epibenthic/benthic species, asymmetric species, or almost symmetric species, which distinguished them from the symmetrical epibenthic/benthic species, namely, *P. leve*, *P. foraminosum*, *P. concavum*, *P. consutum*, *P. bimaculatum*, *P. hoffmannianum* and *P. lima*.

The phylogeny inferred from the ITS region revealed that the species were classified into two clades (Fig. 3). The first clade primarily comprised symmetric epibenthic/benthic species: *P. hoffmannianum*, *P. caipirignum*, *P. lima*, *P. foraminosum*, *P. leve*

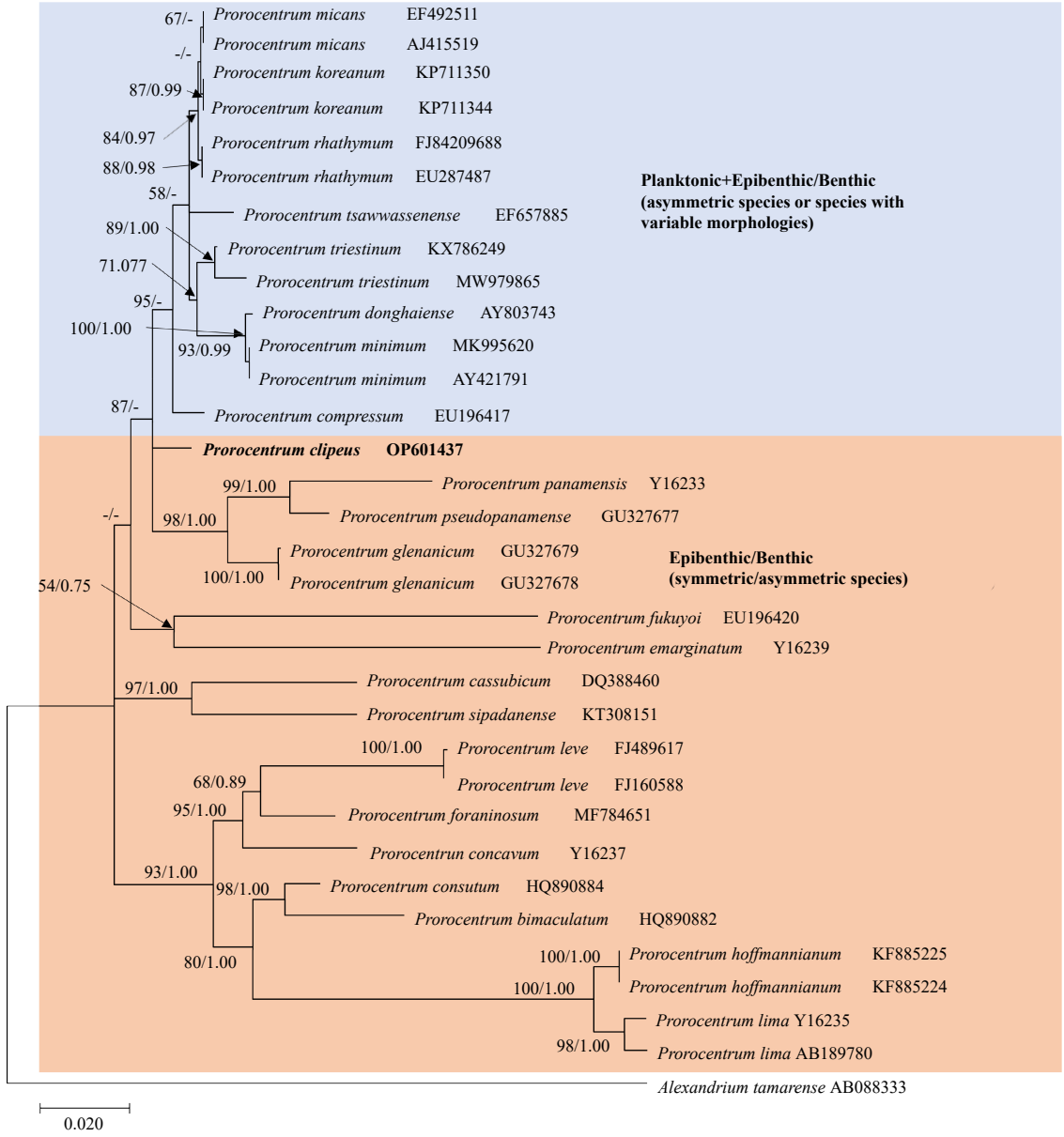

Fig. 2. Maximum likelihood tree of 33 SSU rDNA sequences and 1 691 positions. *Alexandrium tamarense* was included as an outgroup. The best model, chosen by MrModel-Test2.3, was GTR+I+G. The support values shown were obtained by ML and BI. Only values larger than 50% (ML) and 0.50 (BI) are shown. A new sequence published in this study is displayed in bold (OP601437).

and *P. concavum*. It also included several nearly symmetric and asymmetric epibenthic/benthic species, such as *P. borbonicum*, *P. cassubicum*, *P. fukuyoi, P. emarginatum, P. panamense* and *P. clipeus.* This clade formed a highly supported group (ML bootstrap support value: 97; Bayesian posterior probability: 1.00). The other clade comprised planktonic and epibenthic/benthic species; asymmetric species; or species with variable valve morphologies, *P. elegans*, *P. donghaiense*, *P. minimum*, *P. triestinum*, *P. rhathymum*, *P. koreanum* and *P. micans*, which clustered together with a well-supported value of 98/0.86.

According to the LSU rDNA tree (Fig. 4), the earliest diverging lineage within the *Prorocentrum* clades was *P. emarginatum*, followed by *P. sculptile* and *P. fukuyoi*, all of which are asymmetric epibenthic/benthic species. The species *P. clipeus* branched with weak support within a group that included planktonic and epibenthic/benthic species; asymmetric species; or species with variable valve morphology, namely, *P. micans*, *P. koreanum*, *P. rhathymum*, *P. triestinum*, *P. minimum*, *P. donghaiense*, *P. elegans*, *P. tsawwassenense* and *P. compressum*. *Prorocentrum panamense* and *P. glenanicum* formed the sister clade to this group. These species were distinct from the symmetrical and nearly symmetric epibenthic/benthic species, namely, *P. foraminosum*, *P. leve*, *P. concavum*, *P. bimaculatum*, *P. consutum*, *P. lima*, *P. hoffmannianum*, *P. caipirignum*, *P. cassubicum*, *P. sipadanese* and *P. borbonicum.*

The *P. clipeus* strain DF128 differed from that found in France at 39 positions (94.40% similarity, Table 4). Phylogenetic analyses revealed that *P. clipeus* from the Yellow Sea formed a sister clade to those from France with maximal support. The LSU rDNA sequence revealed that the DF128 strain was most closely related to *P. compressum*, with 86.37% similarity, followed by *P. tsawwassenense*, with 79.91% similarity.

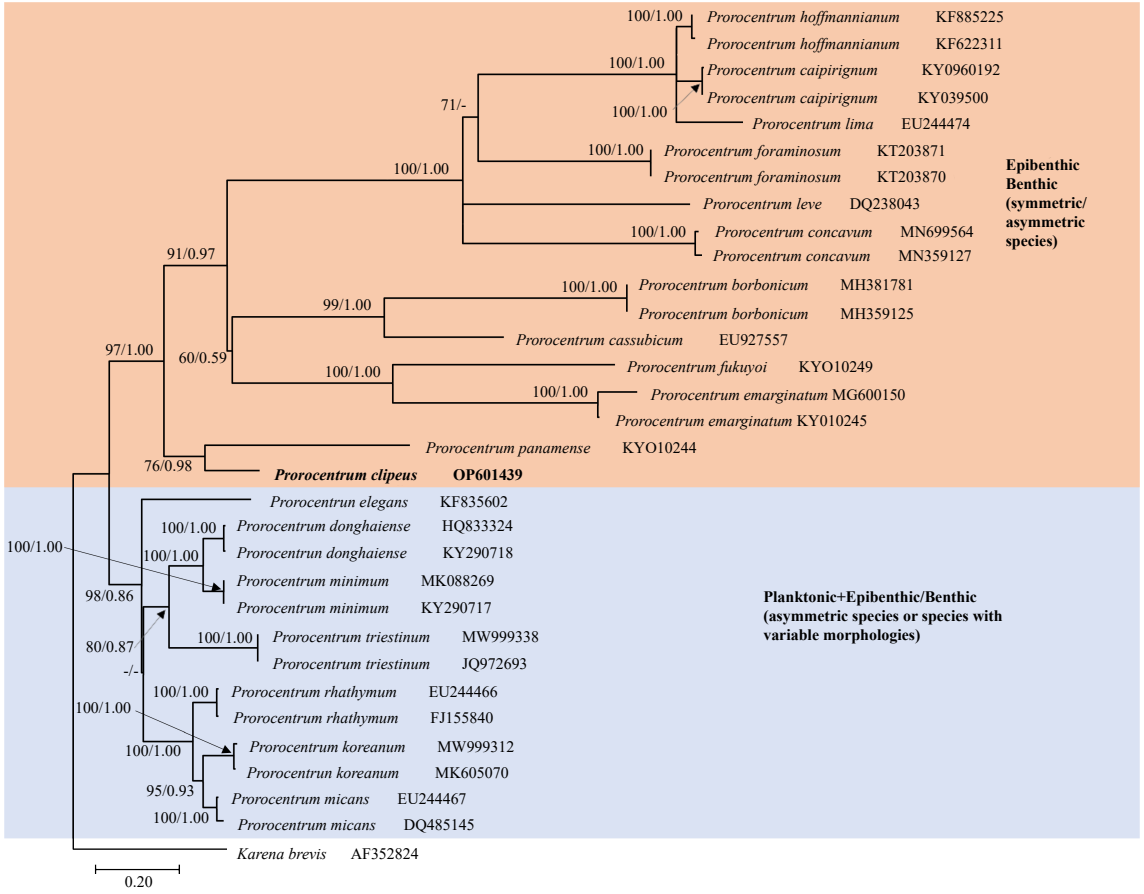

Fig. 3. Maximum likelihood tree of 32 ITS1–5.8S–ITS2 sequences and 623 positions. *Karenia brevis* was included as an outgroup. The best model, chosen by MrModel-Test2.3, was GTR+I+G. The support values shown were obtained by ML and BI. Only values larger than 50% (ML) and 0.50 (BI) are shown. A new sequence published in this study is displayed in bold (OP601439).

3.3 *Metabolite profiling of Prorocentrum clipeus DF128*

According to the results of the target screening, the four toxins OA, DTX1, DTX2 and PTX2 were not detected in the extracts of *P. clipeus* DF128, as shown by the extracted ion chromatograms (EICs) presented in Figs 5 and 6. According to the non-target screening results, 179 previously reported compounds from the DSP-related algal species *Prorocentrum* spp. and *Dinophysis* spp., including OA, DTX1, DTX2 and PTX2, were also not detected. During non-target screening, the FBMN was applied to visualize the metabolome and facilitate the annotation of analytes as metabolites. The constructed molecular network was subsequently annotated using the MolNetEnhancer workflow with the GNPS Library Search tool. An overview of the molecular network generated using positive and negative ion mode mass spectrometric data revealed that the positive ion mode molecular network consisted of 1 252 nodes in 136 clusters (with a minimum of 2 connected nodes) and 973 single nodes, while the negative ion mode molecular network consisted of 657 nodes in 90 clusters and 1 641 single nodes. As detailed in the molecular network, 23 clusters belonging to at least 13 compound classes were identified, and organometallic compounds, lipids and lipid-like molecules, phenylpropanoids and polyketides, and benzenoids were classified as the major convergence points. More metabolites were identified in the positive ion mode molecular network, and lipids and lipid-like molecules (nodes in green) accounted for the majority of both molecular networks (Fig. 7). The nodes representing the standards were not grouped into clusters but were displayed as single nodes in these two molecular networks, suggesting that no analogs of these standards were found in the extracts of *P. clipeus* DF128.

4 Discussion

4.1 *Morphology and biogeography*

The following characteristics of the *Prorocentrum* species analyzed here are consistent with the description of *P. clipeus* by Hoppenrath (2000): (1) the cell shape and size, (2) the type of ornamentation of the thecal plate surface, and (3) the architectural details of the periflagellar area and the intercalary band. Some subtle morphometric differences were observed between the specimens analyzed in this study and those in the original description, with the observed cells being smaller than those described for the first time in isolates from Helgoland, German Bight, North Sea (Hoppenrath, 2000) but consistent with the cell sizes of strains/isolates collected later from Groix Island in France, Port Stephens in Australia, and Jeju Island in Korea (Hoppenrath et al., 2013; Murray, 2003; Shah et al., 2013) (Table 3).

Prorocentrum clipeus and closely related species were compared (Table 3). Considering the cell morphology in the thecal view, *P. clipeus* in this study was more similar to *P. compressum* and *P. tsawwassenense*, being symmetric or slightly asymmetric and round to oval in the lateral view, than to *P. panamense*, which is asymmetric and heart-shaped. Regarding the ornamentation of the thecal plates, *P. clipeus* (in this study, *P. clipeus* DF128) and *P. tsawwassenense* (Hoppenrath et al., 2013; Hop-

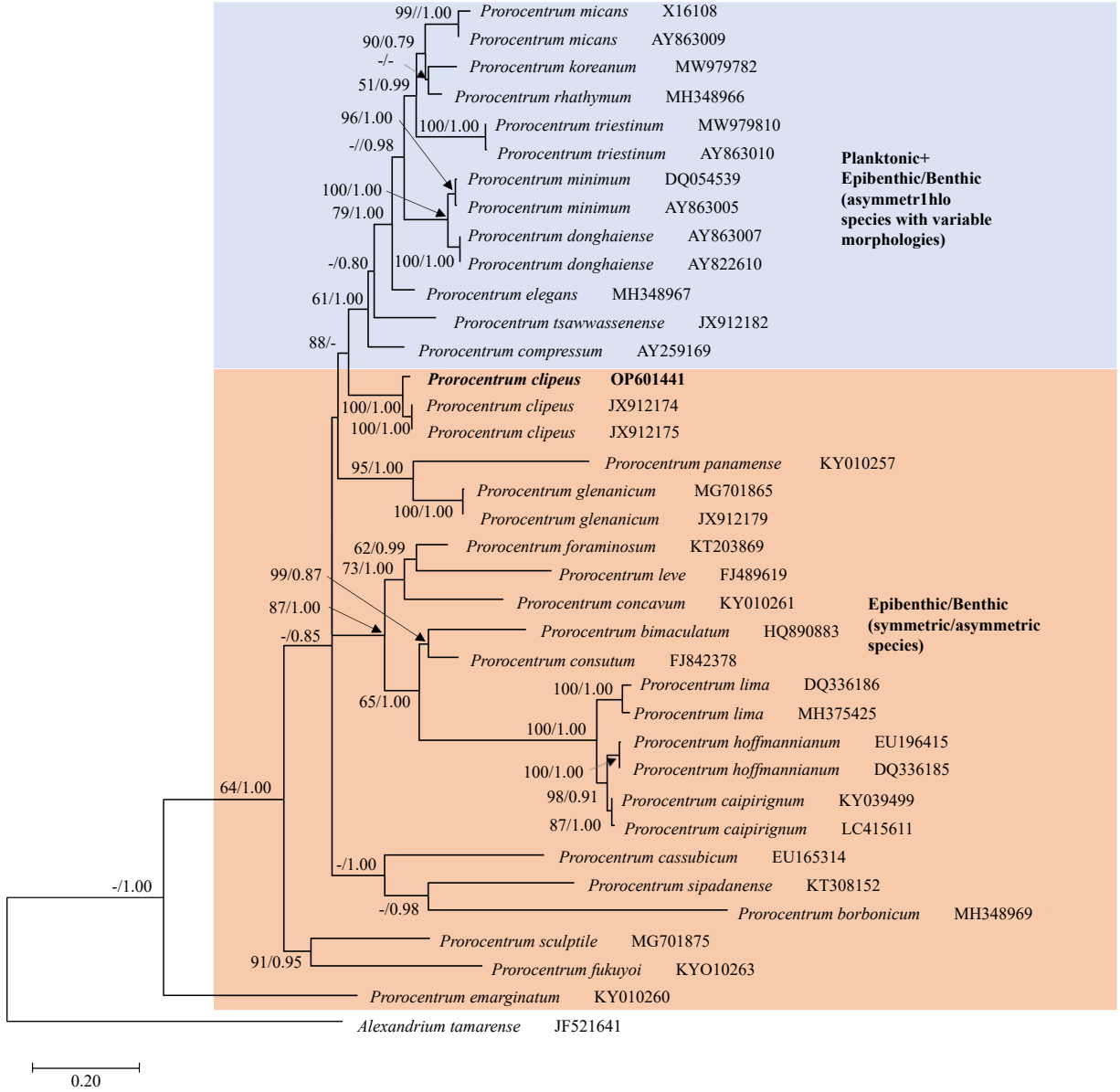

Fig. 4. Maximum likelihood tree of 37 LSU rDNA sequences and 697 positions. *Alexandrium tamarense* was included as an outgroup. The best model, chosen by MrModel-Test2.3, was GTR+I+G. The support values shown were obtained by ML and BI. Only values larger than 50% (ML) and 0.50 (BI) are shown. A new sequence published in this study is displayed in bold (OP601441).

Table 4. LSU rDNA sequence differences (above the diagonal line) and similarities (below the diagonal line) among *P. clipeus*, *P. compressum* and *P. tsawwassenense* based on a total of 697 positions

Species	GenBank No./Strains	Origin	DF128	IFR459	IFR470	PCPA01	IFR456
P. clipeus	OP601441/DF128	China	–	39	39	95	140
P. clipeus	JX912174/IFR459	France	94.4%	–	0	104	121
P. clipeus	JX912175/IFR470	France	94.4%	100%	–	104	121
P. compressum	AY259169/PCPA01	Australia	86.37%	85.08%	85.08%	–	117
P. tsawwassenense	JX912182/IFR456	France	79.91%	82.64%	82.64%	83.21%	–

Note: – represents no data.

penrath and Leander, 2008) are smooth, while *P. panamense* is a reticulate-foveate (Grzebyk et al., 1998; Hoppenrath et al., 2013; Luo et al., 2017), and *P. compressum* is only partially foveate (Gul and Saifullah, 2011). *Prorocentrum clipeus* valves exhibit a visible pore pattern or radial rows of pores, similar to those of *P. tsawwassenense* (Hoppenrath et al., 2013). However, *P. clipeus* has small pores, while *P. tsawwassenense* has both large and small pores on the valve. The periflagellar area of *P. clipeus* is similar to that of *P. tsawwassenense*, with a U-/arc shape (Hoppenrath et al., 2013). *Prorocentrum clipeus* is also similar to *P. tsawwassenense*, with 9 to 10 platelets in the periflagellar area and protrusions on the platelets. However, *P. tsawwassenense* has an

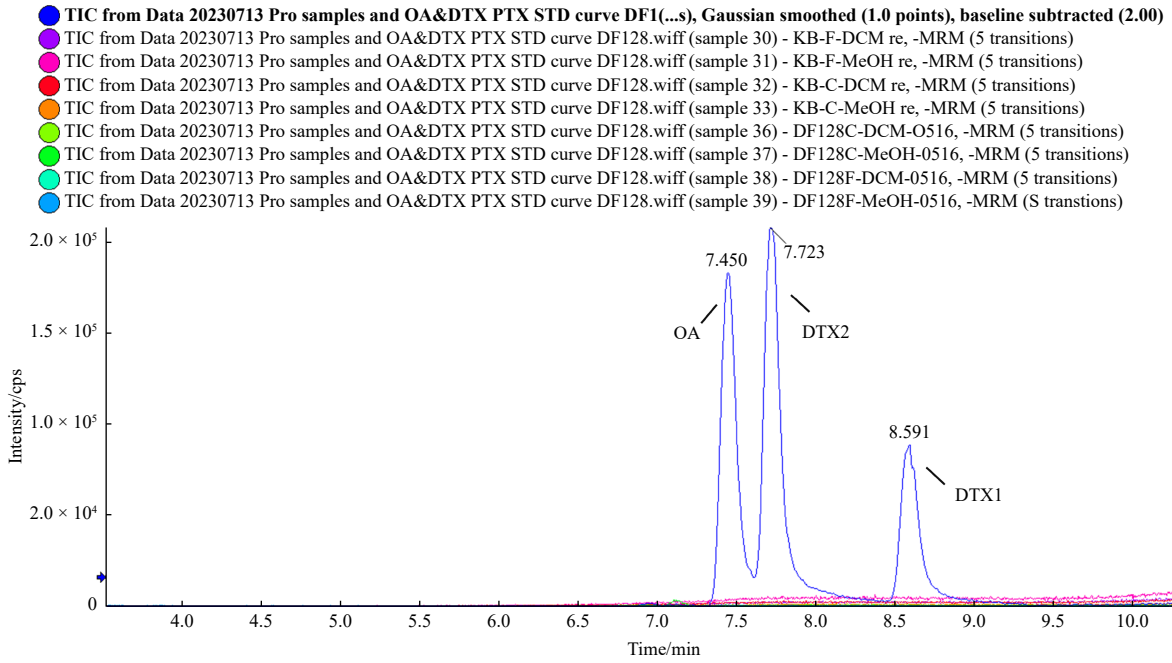

Fig. 5. Extracted ion chromatograms (EICs) of the procedure blank; *P. clipeus* DF128 intracellular and extracellular extracts; and OA, DTX1 and DTX2 standards (100 ng/mL) in negative ESI mode using a Sciex QTRAP 5500 system. cps: count per second.

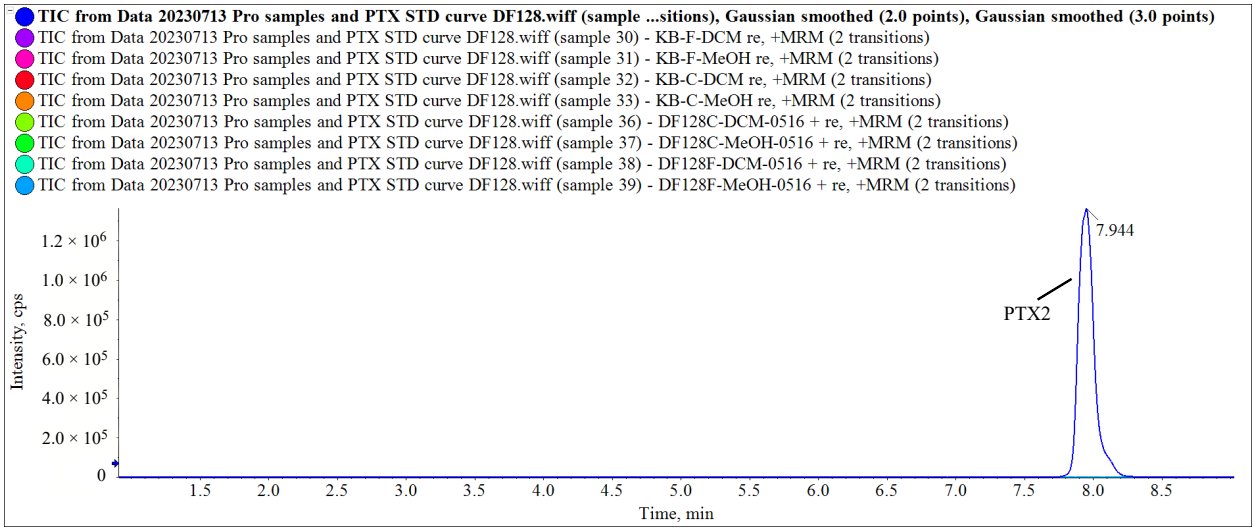

Fig. 6. The EICs of the procedural blank, *P. clipeus* DF128 intracellular and extracellular extracts, and standard PTX2 (100 ng/mL) in positive ESI mode were determined using a Sciex QTRAP 5500 system. cps: count per second.

additional 5–6 protrusions on its platelets and a more variable pattern (Hoppenrath et al., 2013). *Prorocentrum clipeus* has nine periflagellar platelets, with platelet 1 fragmented this study, (Hoppenrath et al., 2013), and has a ridge on the right thecal plate at the edge to the periflagellar area. *Prorocentrum clipeus* differs from all other related species by its wide U-shaped periflagellar area; collar, ridge, and small pores on some platelets; two curved projections on platelet 1; and one protrusion on platelet 8 next to the accessory pore this study, (Hoppenrath et al. 2013).

In the present study, *P. clipeus* was found in different geographical areas. *Prorocentrum clipeus* was first discovered in sandy sediments in cool temperate regions in Germany in 2000. Currently, there are only a few documented reports of the presence of *P. clipeus*. It has been reported in Port Stephens in Australia and in Elba in Italy, as well as on Groix Island in France, Jeju Island in Korea and Thuwal in Saudi Arabia (Hoppenrath, 2000; Hoppenrath et al., 2013, 2014; Prabowo and Agusti, 2019; Shah et al., 2013) (Fig. 8). Additionally, the presence of *P. clipeus* in several locations in South Australia and in estuaries in New South Wales in Australia has been documented in the Ocean Biogeographic Information System (OBIS). *Prorocentrum clipeus* is distributed between 54.18° N and 36.97° S, and it typically inhabits temperate to subtropical coastal areas. It has been reported in the Pacific Ocean, the Atlantic Ocean, the North Sea, the Mediterranean Sea, and the Indian Ocean. It is widely distributed in the Pacific Ocean, including the southeastern coastal waters of Australia. To date, there have been no reports on the distribution of *P. clipeus* in North and South America.

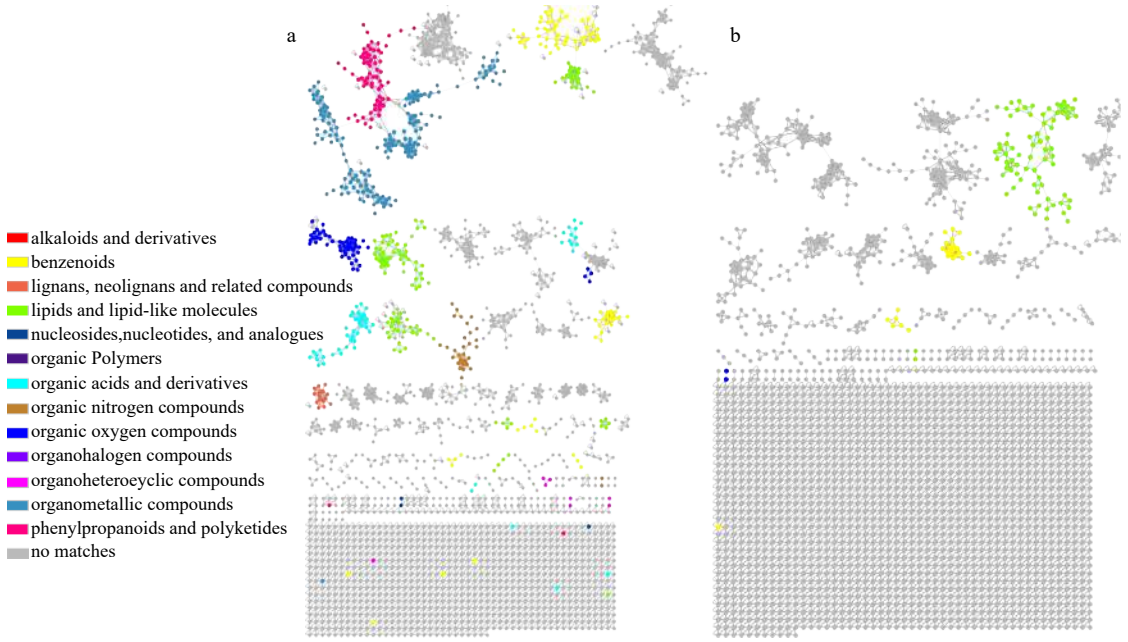

Fig. 7. Enhanced molecular networks obtained from the positive ion mode (a) and negative ion mode (b) mass spectra using MolNetEnhancer showing different molecular families/clusters of the pooled metabolites in the extracts of *P. clipeus* DF128. The node colors represent the classes of putatively annotated metabolites matched in the GNPS libraries. Single nodes indicate the absence of MS/MS fragments shared with any other compound.

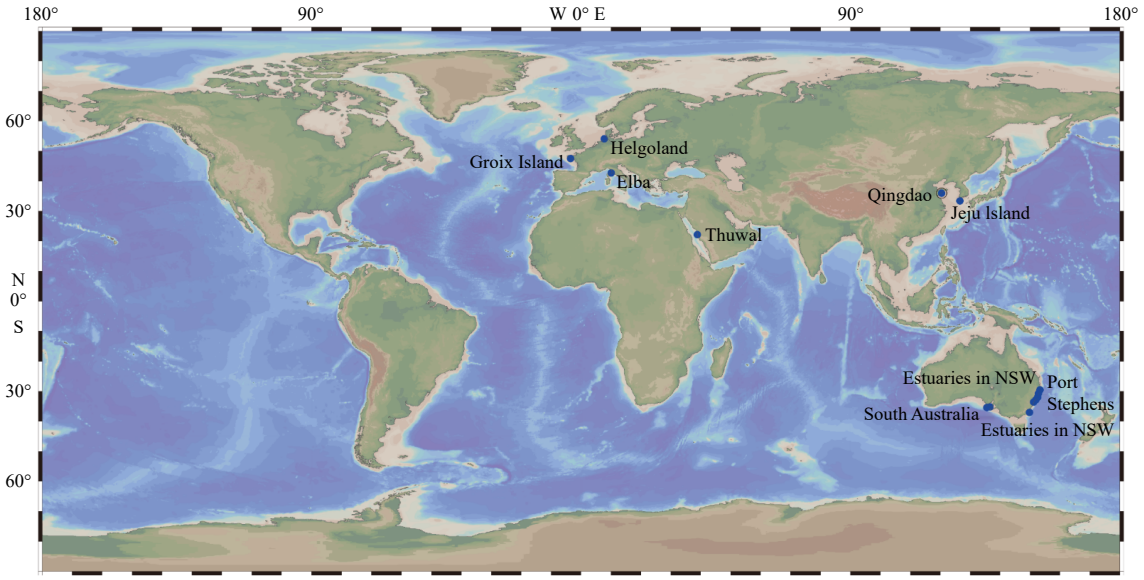

Fig. 8. Global occurrence of *P. clipeus* (data from this paper indicated by double circle marker; data from published literature and OBIS from 2000 to 2019 in black). The figure was created using Ocean Data View, version 5.7.1 (Schlitzer, 2023).

4.2 *Molecular phylogeny*

All the trees showed that *P. clipeus* was clearly separated from the other species, and each subclade had good nodal support. In all the phylogenetic analyses, *P. clipeus* was embedded in groups containing asymmetric and symmetric epibenthic/benthic species (e.g., *P. borbonicum*, *P. caipirignum*, *P. cassubicum*, *P. concavum*, *P. emarginatum*, and *P. fukuyoi*). The results of these analyses were congruent with those of previous studies (Boopathi et al., 2015; Chomérat et al., 2010, 2012; Hoppenrath et al., 2013), which distinguished *Prorocentrum* species by their symmetry. ITS analysis of *Prorocentrum* revealed two distinct clades: one clade consisted of both planktonic and epibenthic/benthic species, including the type species *P. micans*, while the other included only epibenthic/benthic species. The ITS analyses were congruent with those of Borsato et al. (2023), which showed the existence of two major clades. According to all the phylogenetic analyses, *P. clipeus* was related to *P. tsawwassenense* and *P. panamense*. These species were described as having U-/arc-shaped periflagellar area with protrusion(s) or "linear" periflagellar area and asymmetry and were clearly distinguished from species with V-shaped periflagellar area (*P. emarginatum*, *P. fukuyoi* and *P. sculptile*) in the phylogenetic analysis. Our results supported

the idea that the shape of the periflagellar area was phylogenetically significant (Hoppenrath et al., 2013). Although our strain was easily identifiable by SEM analysis and confirmed by phylogenetic analysis, the *P. emarginatum*/*P. fukuyoi* complex and the *P. cassubicum* clade exhibited additional cryptic morphology, leading to confusion, which was evident in all three (SSU, ITS, and LSU) trees. Nevertheless, the small number of sequences available in GenBank allowed us to confirm that strain DF128 belongs to *P. clipeus* via BLAST analysis, and our results will provide additional genetic and phylogenetic information through the subsequent deposition of the SSU and ITS sequences in GenBank.

4.3 *Metabolite profiling*

Information on the toxin contents or metabolite profiles of *P. clipeus* strains found worldwide is currently very limited. To fill this research gap, intracellular and extracellular extracts of *P. clipeus* DF128 were evaluated via target, suspect, and non-target screening under the culture conditions described in this study. The results of both target and suspect screening indicated that no known metabolites or toxins were detected in DSP-related algal species. However, it cannot be concluded whether the obtained *P. clipeus* is toxic. Non-target screening utilizing FBMN provided a comprehensive view of the major metabolites, especially unknown metabolites, which may be congeners of known toxins, complementing target and suspect screenings. Both DSP toxins and PTXs have a polyketide backbone with carboxyl groups, which can be attributed to polyketides and fatty acids (Rein and Snyder, 2006). Polyketides are a large group of structurally diverse acetate-derived natural products, many of which are toxic (Wan et al., 2019). The identification of numerous polyketides and lipids in the current isolate of *P. clipeus* suggested the potential presence of other unknown bioactive polyketides and fatty acids. Thus, metabolite profiling was used in this study to systematically evaluate the potential of DSPs and the presence of other toxins.

5 Conclusions

In this study, we described one benthic species of *Prorocentrum* collected from the Yellow Sea, which was morphologically and phylogenetically identified as *P. clipeus*. In addition to the shape of cells, *P. clipeus* can be distinguished from other species in the genus by its unique morphological structure. The target and suspect screening results revealed no known metabolites or toxins in the *P. clipeus* DF128 samples, suggesting the relatively low risk potential of this species in the marine environment. Non-target screening identified more metabolites in the positive ion mode molecular network than in the negative ion mode molecular network, and lipids and lipid-like molecules accounted for the majority of both the positive and negative ion mode molecular networks. Although OA and its analogs were not detected in this study, the identification of polyketides and lipids indicates the potential toxicity of the obtained *P. clipeus* strain. Furthermore, we updated the known global distribution of the genus *Prorocentrum*, providing crucial information for further elucidating the ecological role and associated risks of this genus.

References

Andersen R A. 2005. Algal Culturing Techniques. Oxford: Elsevier Academic Press, 578

Arteaga-Sogamoso E, Rodríguez F, Amato A, et al. 2023. Morphology and phylogeny of *Prorocentrum porosum* sp. nov. (Dinophyceae): a new benthic toxic dinoflagellate from the Atlantic and Pacific Oceans. Harmful Algae, 121: 102356, doi: 10.1016/j.hal.2022.102356

Blanco J, Moroño Á, Fernández M L. 2005. Toxic episodes in shellfish, produced by lipophilic phycotoxins: an overview. Galician: Revista Galega dos Recursos Mariños Galician Journal of Marine Resources, 1: 1–70

Boopathi T, Faria D G, Cheon J Y, et al. 2015. Implications of high molecular divergence of nuclear rRNA and phylogenetic structure for the dinoflagellate *Prorocentrum* (Dinophyceae, Prorocentrales). Journal of Eukaryotic Microbiology, 62(4): 519–531, doi: 10.1111/jeu.12206

Borsato G T, Salgueiro F, De'Carli G A L, et al. 2023. Taxonomy and abundance of epibenthic *Prorocentrum* (Dinophyceae) species from the tropical and subtropical Southwest Atlantic Ocean including a review of their global diversity and distribution. Harmful Algae, 127: 102470, doi: 10.1016/j.hal.2023.102470

Chomérat N, Bilien G, Zentz F. 2019. A taxonomical study of benthic *Prorocentrum* species (Prorocentrales, Dinophyceae) from Anse Dufour (Martinique Island, eastern Caribbean Sea). Marine Biodiversity, 49(3): 1299–1319, doi: 10.1007/s12526-018-0913-6

Chomérat N, Saburova M, Bilien G, et al. 2012. *Prorocentrum bimaculatum* sp. nov. (Dinophyceae, Prorocentrales), a new benthic dinoflagellate species from Kuwait (Arabian Gulf). Journal of Phycology, 48(1): 211–221, doi: 10.1111/j.1529-8817.2011.01102.x

Chomérat N, Sellos D Y, Zentz F, et al. 2010. Morphology and molecular phylogeny of *Prorocentrum consutum* sp. nov. (Dinophyceae), a new benthic dinoflagellate from south brittany (northwestern France). Journal of Phycology, 46(1): 183–194, doi: 10.1111/j.1529-8817.2009.00774.x

Chomérat N, Zentz F, Boulben S, et al. 2011. *Prorocentrum glenanicum* sp. nov. and *Prorocentrum pseudopanamense* sp. nov. (Prorocentrales, Dinophyceae), two new benthic dinoflagellate species from South Brittany (northwestern France). Phycologia, 50(2): 202–214, doi: 10.2216/10-12.1

Dodge J D. 1975. The Prorocentrales (Dinophyceae). II. Revision of the taxonomy within the genus *Prorocentrum*. Botanical Journal of the Linnean Society, 71(2): 103–125, doi: 10.1111/j.1095-8339.1975.tb02449.x

Ehrenberg C. 1834. Dritter beitrag zur erkenntniss grosser organisation in der richtung des kleinsten raumes. Berlin: Abhandlungen der Königlichen Akademie der Wissenschaften zu, 1833: 145–336

Ernst M, Kang K B, Caraballo-Rodríguez A M, et al. 2019. MolNetEnhancer: enhanced molecular networks by integrating metabolome mining and annotation tools. Metabolites, 9(7): 144, doi: 10.3390/metabo9070144

European Food Safety Authority. 2008. Marine biotoxins in shellfish - okadaic acid and analogues - scientific opinion of the panel on contaminants in the food chain. European Food Safety Authority Journal, 6(1): 589, doi: 10.2903/j.efsa.2008.589

Faust M A, Vandersea M W, Kibler S R, et al. 2008. *Prorocentrum levis*, a new benthic species (Dinophyceae) from a mangrove island, Twin Cays, Belize. Journal of Phycology, 44(1): 232–240, doi: 10.1111/j.1529-8817.2007.00450.x

Freudenthal A, Jijina J. 1988. Potential hazards of *Dinophysis* to consumers and shellfisheries. Journal of Shellfish Research, 7(1): 157–158

Fu X H, Meng F L, Hu Y, et al. 2008. *Candida albicans*, a distinctive fungal model for cellular aging study. Aging Cell, 7(5): 746–757, doi: 10.1111/j.1474-9726.2008.00424.x

Glibert P M, Burkholder J M, Kana T M. 2012. Recent insights about relationships between nutrient availability, forms, and stoichiometry, and the distribution, ecophysiology, and food web effects of pelagic and benthic *Prorocentrum* species. Harmful Algae, 14: 231–259, doi: 10.1016/j.hal.2011.10.023

Gómez F, Gourvil P, Li T C, et al. 2023. Molecular phylogeny of the spiny - surfaced species of the dinoflagellate *Prorocentrum* with the description of *P. thermophilum* sp. nov. and *P. criophilum* sp. nov. (Prorocentrales, Dinophyceae). Journal of Phycology, 59(1): 70–86, doi: 10.1111/jpy.13298

Grzebyk D, Sako Y, Berland B. 1998. Phylogenetic analysis of nine species of *Prorocentrum* (Dinophyceae) inferred from 18S ribosomal DNA sequences, morphological comparisons, and description of *Prorocentrum panamensis*, sp. nov. Journal of Phycology, 34(6): 1055–1068, doi: 10.1046/j.1529-8817.1998.341055.x

Gul S, Saifullah S M. 2011. The dinoflagellate genus *Prorocentrum* (Prorocentrales, Prorocentraceae) from the north Arabian sea. Pakistan Journal of Botany, 43(6): 3061–3065

Gurevich A, Mikheenko A, Shlemov A, et al. 2018. Increased diversity of peptidic natural products revealed by modification-tolerant database search of mass spectra. Nature Microbiology, 3(3): 319–327, doi: 10.1038/s41564-017-0094-2

Hall T A. 1999. BioEdit: a user-friendly biological sequence alignment editor and analysis program for Windows 95/98/NT. Nucleic Acids Symposium Series, 41: 95–98

Han M S, Wang Pengbin, Kim J H, et al. 2016. Morphological and molecular phylogenetic position of *Prorocentrum micans* sensu stricto and description of *Prorocentrum koreanum* sp. nov. from southern coastal waters in Korea and Japan. Protist, 167(1): 32–50, doi: 10.1016/j.protis.2015.12.001

Henrichs D W, Scott P S, Steidinger K A, et al. 2013. Morphology and phylogeny of *Prorocentrum texanum* sp. nov. (Dinophyceae): a new toxic dinoflagellate from the Gulf of Mexico coastal waters exhibiting two distinct morphologies. Journal of Phycology, 49(1): 143–155, doi: 10.1111/jpy.12030

Holman J D, Tabb D L, Mallick P. 2014. Employing ProteoWizard to convert raw mass spectrometry data. Current Protocols in Bioinformatics, 46(1): 13.24. 1–13.24. 9, doi: 10.1002/0471250953.bi1324s46

Hong D D, Thu N T H, Nam H S, et al. 2008. The phylogenetic tree of *Alexandrium, Prorocentrum* and *Pseudo-nitzschia* of harmful and toxic algae in vietnam coastal waters based on sequences of 18s rDNA, ITS1-5.8S-ITS2 gene fragments and single cell-PCR method. Marine Research in Indonesia, 32(2): 203–218, doi: 10.14203/mri.v32i2.456

Hoppenrath M. 2000. A new marine sand-dwelling *Prorocentrum* species, *P. clipeus* sp. nov. (Dinophyceae, Prorocentrales) from Helgoland, German Bight, North Sea. European Journal of Protistology, 36(1): 29–33, doi: 10.1016/S0932-4739(00)80019-X

Hoppenrath M, Chomérat N, Horiguchi T, et al. 2013. Taxonomy and phylogeny of the benthic *Prorocentrum* species (Dinophyceae)—a proposal and review. Harmful Algae, 27: 1–28, doi: 10.1016/j.hal.2013.03.006

Hoppenrath M, Leander B S. 2008. Morphology and molecular phylogeny of a new marine sand-dwelling *Prorocentrum* species, *P. tsawwassenense* (Dinophyceae, Prorocentrales), from British Columbia, Canada. Journal of Phycology, 44(2): 451–466, doi: 10.1111/j.1529-8817.2008.00483.x

Hoppenrath M, Murray S A, Chomérat N, et al. 2014. Marine Benthic Dinoflagellates-Unveiling Their Worldwide Biodiversity. Stuttgart: Senckenberg, 137–138

Keller M D, Selvin R C, Claus W, et al. 1987. Media for the culture of oceanic ultraphytoplankton. Journal of Phycology, 23(4): 633–638, doi: 10.1111/j.1529-8817.1987.tb04217.x

Jackson A E, Marr J C, Mclachlan J L. 1993. The production of diarrhetic shellfish toxins by an isolate of *Prorocentrum lima* from Nova Soctia, Canada. In: Smayda TJ, Shimizu Y, eds. Toxic Phytoplankton Blooms in the Sea. Newport: Elsevier, 513–518

Lim Z F, Luo Zhaohe, Lee L K, et al. 2019. Taxonomy and toxicity of *Prorocentrum* from Perhentian Islands (Malaysia), with a description of a non-toxigenic species *Prorocentrum malayense* sp. nov. (Dinophyceae). Harmful Algae, 83: 95–108, doi: 10.1016/j.hal.2019.01.007

Luo Zhaohe, Zhang Hua, Krock B, et al. 2017. Morphology, molecular phylogeny and okadaic acid production of epibenthic *Prorocentrum* (Dinophyceae) species from the northern South China Sea. Algal Research, 22: 14–30, doi: 10.1016/j.algal.2016.11.020

Mohimani H, Gurevich A, Shlemov A, et al. 2018. Dereplication of microbial metabolites through database search of mass spectra. Nature Communications, 9(1): 4035, doi: 10.1038/s41467-018-06082-8

Murray S. 2003. Diversity and phylogenetics of sand-dwelling dinoflagellates from southern Australia [dissertation]. Sydney: University of Sydney

Murray S, Nagahama Y, Fukuyo Y. 2007. Phylogenetic study of benthic, spine-bearing prorocentroids, including *Prorocentrum fukuyoi* sp. nov. Phycological Research, 55(2): 91–102, doi: 10.1111/j.1440-1835.2007.00452.x

Nascimento S M, Mendes M C Q, Menezes M, et al. 2017. Morphology and phylogeny of *Prorocentrum caipirignum* sp. nov. (Dinophyceae), a new tropical toxic benthic dinoflagellate. Harmful Algae, 70: 73–89, doi: 10.1016/j.hal.2017.11.001

Nothias L F, Petras D, Schmid R, et al. 2020. Feature-based molecular networking in the GNPS analysis environment. Nature Methods, 17(9): 905–908, doi: 10.1038/s41592-020-0933-6

Olmos-Soto J, Paniagua-Michel J, Contreras R, et al. 2002. Molecular identification of β-carotene hyper-producing strains of *Dunaliella* from saline environments using species-specific oligonucleotides. Biotechnology Letters, 24(5): 365–369, doi: 10.1023/A:1014516920887

Prabowo D A, Agusti S. 2019. Free-living dinoflagellates of the central Red Sea, Saudi Arabia: Variability, new records and potentially harmful species. Marine Pollution Bulletin, 141: 629–648, doi: 10.1016/j.marpolbul.2019.03.012

Rein K S, Snyder R V. 2006. The biosynthesis of polyketide metabolites by dinoflagellates. Advances in Applied Microbiology, 59: 93–125, doi: 10.1016/S0065-2164(06)59004-5

Ronquist F, Teslenko M, Van Der Mark P, et al. 2012. MrBayes 3.2: efficient Bayesian phylogenetic inference and model choice across a large model space. Systematic Biology, 61(3): 539–542, doi: 10.1093/sysbio/sys029

Schlitzer R. 2023. Ocean data view. http://odv.awi.de

Schmid R, Heuckeroth S, Korf A, et al. 2023. Integrative analysis of multimodal mass spectrometry data in MZmine 3. Nature Biotechnology, 41(4): 447–449, doi: 10.1038/s41587-023-01690-2

Scholin C A, Herzog M, Sogin M, et al. 1994. Identification of group - and strain - specific genetic markers for globally distributed *Alexandrium* (Dinophyceae). II. Sequence analysis of a fragment of the LSU rRNA gene. Journal of Phycology, 30(6): 999–1011, doi: 10.1111/j.0022-3646.1994.00999.x

Shah M M R, An S J, Lee J B. 2013. Presence of benthic dinoflagellates around coastal waters of Jeju Island including newly recorded species. Journal of Ecology and Environment, 36(4): 347–370, doi: 10.5141/ecoenv.2013.347

Shannon P, Markiel A, Ozier O, et al. 2003. Cytoscape: a software environment for integrated models of biomolecular interaction networks. Genome Research, 13(11): 2498–2504, doi: 10.1101/gr.1239303

Swofford D L, 2002. PAUP: phylogenetic analysis using parsimony, version 4.0 b10. Sinauer Associates, Sunderland, MA

Ten-Hage L, Turquet J, Quod J P, et al. 2000. *Prorocentrum borbonicum* sp. nov. (Dinophyceae), a new toxic benthic dinoflagellate from the southwestern Indian Ocean. Phycologia, 39(4): 296–301, doi: 10.2216/i0031-8884-39-4-296.1

Thompson J D, Higgins D G, Gibson T J. 1994. CLUSTAL W: improving the sensitivity of progressive multiple sequence alignment through sequence weighting, position-specific gap penalties and weight matrix choice. Nucleic acids research, 22(22): 4673–4680, doi: 10.1093/nar/22.22.4673

Tillmann U, Gottschling M, Wietkamp S, et al. 2023a. Morphological and phylogenetic characterisation of *Prorocentrum spinulentum*, sp. nov. (Prorocentrales, Dinophyceae), a small spiny species from the North Atlantic. Microorganisms, 11(2): 271, doi: 10.3390/microorganisms11020271

Tillmann U, Hoppenrath M, Gottschling M. 2019. Reliable determination of *Prorocentrum micans* Ehrenb. (Prorocentrales, Dinophyceae) based on newly collected material from the type locality. European Journal of Phycology, 54(3): 417–431, doi: 10.1080/09670262.2019.1579925

Tillmann U, Wietkamp S, Gottschling M, et al. 2023b. *Prorocentrum pervagatum* sp. nov. (Prorocentrales, Dinophyceae): a new, small, planktonic species with a global distribution. Phycologic-

al Research, 71(1): 56–71, doi: 10.1111/pre.12502
Verma A, Kazandjian A, Sarowar C, et al. 2019. Morphology and phylogenetics of benthic *Prorocentrum* Species (Dinophyceae) from tropical northwestern Australia. Toxins, 11(10): 571, doi: 10.3390/toxins11100571
Wan Xiukun, Yao Ge, Liu Yanli, et al. 2019. Research progress in the biosynthetic mechanisms of marine polyether toxins. Marine Drugs, 17(10): 594, doi: 10.3390/md17100594
Wu Yixuan, Huang Shuning, Krock B, et al. 2022. Cryptic speciation of benthic *Prorocentrum* (Dinophyceae) species and their potential as ecological indicators. Journal of Sea Research, 190: 102304, doi: 10.1016/j.seares.2022.102304
White T J, Bruns T, Lee S, et al. 1990. Amplification and direct sequencing of fungal ribosomal RNA genes for phylogenetics. In: Innis M A, Gelfand D H, Sninsky J J, et al, eds. PCR Protocols: A Guide to Methods and Applications. New York: Academic Press, 315–322, doi: 10.1016/B978-0-12-372180-8.50042-1
Xie Hang, Zou Jian, Zheng Chengzhi, et al. 2022. Biodiversity and distribution of benthic dinoflagellates in tropical Zhongsha Islands, South China Sea. Journal of Oceanology and Limnology, 40(6): 2120–2145, doi: 10.1007/s00343-022-1322-z
Yasumoto T, Murata M, Oshima Y, et al. 1985. Diarrhetic shellfish toxins. Tetrahedron, 41(6): 1019–1025, doi: 10.1016/S0040-4020(01)96469-5
Zhang Hua, Li Yang, Cen Jingyi, et al. 2015. Morphotypes of *Prorocentrum lima* (Dinophyceae) from Hainan island, South China Sea: morphological and molecular characterization. Phycologia, 54(5): 503–516, doi: 10.2216/15-8.1
Zou Jian, Li Qun, Liu Hui, et al. 2022. Taxonomy and toxin profile of harmful benthic *Prorocentrum* (Dinophyceae) species from the Xisha Islands, South China Sea. Journal of Oceanology and Limnology, 40(3): 1171–1190, doi: 10.1007/s00343-021-1045-6
Zou Jian, Li Qun, Lu Songhui, et al. 2020. The first benthic harmful dinoflagellate bloom in China: morphology and toxicology of *Prorocentrum concavum*. Marine Pollution Bulletin, 158: 111313, doi: 10.1016/j.marpolbul.2020.111313